Efficiency Maximization of the Air Core Double-Sided Permanent Magnet Linear Synchronous Motor

A. Darabi[1], R. Ghanaee[1], A. Shariati[1], M. Siahi[1]
[1]Electrical Engineering Department, Azad University,
Garmsar Branch, Garmsar, Iran
darabi_ahmad@hotmail.com

Abstract—**Air core permanent magnet linear synchronous motor (ACPMLSM) recommended for applications in which the accurate control of speed and position is required. Omission of the core in the primary of the motor reduces the detent force and increases the controllability of the motor. In this paper, the flux density of different parts of an ACPMLSM is calculated using both the Maxwell's equations and finite element method (FEM). A precise flux density model is presented and the design of the air core double sided permanent magnet linear synchronous motor is optimized for the efficiency maximization using the genetic algorithm method.**

Index Terms—**Air core permanent magnet linear synchronous motor, flux density, efficiency, genetic algorithm, finite element method.**

I. INTRODUCTION

The permanent magnet linear synchronous motors (PMLSM) have taken more attention than linear induction motors because of high force density and efficiency, low losses, satisfactory dynamic performance and easy control [1]–[6]. However, the detent force generated by the slotted structure and the end effect caused by the limited length of the moving part are the main disadvantages of slotted linear motors. Some techniques such as skewing the slots and optimizing the permanent magnet (PM) and the width of the primary winding have been already suggested to reduce the detent force [5]–[7]. Position and speed control of a PMLSM can be improved by mitigation or alleviation of the detent force. Since using the air-core instead of the iron core in a permanent magnet linear synchronous motor considerably reduces the detent force; the air core machine is usually recommended for high precise applications.

Some investigations are carried out on the optimal design of the PMLSM. It has been shown that some increases in the thrust can be achieved by modifying the shape or dimension of the permanent magnet and width of the winding [7], [8]. The ripple reduction has been the other concern of earlier studies [7]. Authors in [9], have been optimized the motor design in order to reduce the electrical time constant. In [10] increasing the motor thrust and reducing the magnet

consumption have been the goals for the optimization. In [11], the output power maximization or loss minimization has been done for a tubular permanent magnet linear synchronous motor.
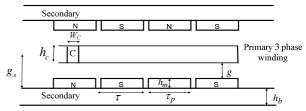
In general, the efficiency of a small PMLSM employed in a control system, is not considered as the main objective, and so the most efforts as mentioned earlier have been conducted to improve the transient responses of the machine. However, the efficiency is one of the most important criteria when employing a motor for the energy conversion purposes. Due to the increasingly development of the linear motors in the industry, the efficiency optimization needs more attention.

In this paper, efficiency optimization of a four pole ACPMLSM is investigated. The paper is organized as the following: in section 2, the basic structure of the ACPMLSM is presented and the procedures to evaluate the air gap flux density distribution are discussed. The flux density distributions are obtained by the use of both Maxwell equations as an analytical method and the finite element method as a numerical method. Finally, a comparison between the results is given in section 2. Section 3 involves the design formulations and modelling tasks of the ACPMLSM defining the existing relationships among some performance characteristics and the design parameters. The optimization algorithm and the results are presented in section 4. Finally, the conclusion and discussion are presented in section 5.

II. FLUX DENSITY DISTRIBUTION OF ACPMLSM

A. Motor structure

The structure of an ACPMLSM is shown in Fig. 1 in which the moving part of motor is a short primary and consists of a three phase air core winding.

Fig. 1. The structure of ACPMLSM.

The secondary part involves the N and S permanent magnets located on the surfaces of the back irons. The primary and the secondary parts are separated by an air gap g. The parameters and the dimensions of the motor are presented in Table I.

Supposing that the primary winding is not excited, an ACPMLSM, as shown in Fig. 2, contains two layers of iron extended along x axis, two layers of PMs and a layer of air gap.

The following assumptions are made for the magnetic field calculation [3], [4]:

1) All the regions (shown in Fig. 2) are extended along $\pm x$;
2) The end effects along z axis are neglected;
3) The permeability of the PM is considered equal to vacuum permeability μ_0;
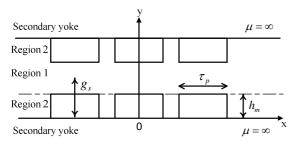4) The permeability of the secondary yoke is infinite.

Fig. 2. Analysis model of an ACPMLSM.

TABLE I. PARAMETERS OF THE STUDIED MOTOR.

Parameter	Symbol	Value
Number of turns	N_1	528
Height of the secondary yoke	h_b	10 mm
Width of the motor	L	100 mm
Pole pitch	τ	46.5 mm
Residual flux density	Br	1.2 Tesla
Width of the PM	τ_p	40 mm
Height of the PM	hm	5 mm
Height of the winding	hc	12 mm
Air gap length	g	0.5 mm
Width of the winding	w_c	15.5 mm
Relative permeability of PM	μ_r	1.05

B. Flux density distribution

Considering Coulomb criteria, $\nabla.A = 0$, Maxwell's equations to calculate the magnetic potential of the PMs can be expressed by Laplace and Poisson partial differential equations as below [4]:

$$\begin{cases} \dfrac{\partial^2 A_1}{\partial x^2} + \dfrac{\partial^2 A_1}{\partial y^2} = 0, \\ \\ \dfrac{\partial^2 A_2}{\partial x^2} + \dfrac{\partial^2 A_2}{\partial y^2} = -\mu_0 J_2, \end{cases} \tag{1}$$

where A is the magnetic vector potential. Flux density B is obtained by using the vector potential as

$$B = \nabla \times A. \tag{2}$$

The subscripts determine the regions and J_2 is the equivalent current density defining the whole permanent magnet effects that can be expressed as the Fourier series [4]

$$J_2 = \sum_{n=1,3,...}^{\infty} \alpha_n \sin(nkx) \tag{3}$$

with coefficients

$$\alpha_n = -\frac{4B_r}{\tau\mu_0}\sin\left(\frac{1}{2}nk\tau_p\right), \tag{4}$$

where $k = \pi/\tau$ is the spatial frequency. Considering Maxwell's equations ($\nabla \times H = J$), the boundary condition that must be satisfied at the border surface of two materials is as below [4]

$$\hat{n} \times (H_1 - H_2) = 0, \tag{5}$$

where $\hat{n}$ is a unit vector normal to the boundary surface directed from region 2 to region 1 and H is the magnetic field intensity. Equation (5) can be expressed as below [4]:

$$\begin{cases} H_{1x} = 0, & y = g_s, \\ H_{1x} = H_{2x} \ and \ B_{1y} = B_{2y}, \ y = h_m, \\ H_{2x} = 0, & y = 0. \end{cases} \tag{6}$$

Given the boundary conditions (6) and the excitation J_2 the X-Y components of the flux density can be expressed as below [4]:

$$B_{1x} = -\mu_0 \sum_{n=1,3,...}^{\infty} \frac{\alpha_n}{(nk)} \cdot \left(\frac{\sinh(nkh_m)}{\sinh(nkg_s)}\sinh(nk(g_s - y))\right) \times \\ \times \sin(nkx), \tag{7}$$

$$B_{1y} = -\mu_0 \sum_{n=1,3,...}^{\infty} \frac{\alpha_n}{(nk)} \cdot \left(\frac{\sinh(nkh_m)}{\sinh(nkg_s)}\cosh(nk(g_s - y))\right) \times \\ \times \cos(nkx). \tag{8}$$

In the rest of this section, the flux density of the primary winding is calculated using the method in [1]. In this method, at the first step the magnetic potential of the primary winding A_s is calculated based on the magneto motive force (MMF) of the traveling magnetic field. At the next step, the distribution of the flux density B_s is calculated using the magnetic potential. According to the method in [1], the amplitude of the vth harmonic of MMF produced by the primary winding is equal to

$$f_{sv} = \frac{6\sqrt{2}}{\pi p K_c} N_1 I_a \frac{1}{v} k_{wv}, \tag{9}$$

where I_a is the RMS value of the phase current, p is the number of pole pairs, k_{wv} is the winding factor for the vth harmonic and K_c is the Carter's coefficient.

According to Laplace equation and the boundary conditions the components of the flux density generated by the primary winding in the middle of the air gap can be expressed as follows:

$$\begin{cases} A_{s1} = 0 \;, & y = h_m + g \;, \\ A_{s1} = f_{sv}, & y = g_s \;. \end{cases} \quad (10)$$

$$B_{s1x} = -\mu_0 \frac{\partial A_{s1}}{\partial x} =$$

$$= -\mu_0 \sum_{v=1}^{\infty} \frac{\pi}{v\tau} f_{sv} \frac{\sinh\left[\frac{v\pi}{\tau}(h_m + g - y)\right]}{\sinh\left[\frac{v\pi}{\tau}(h_m + g)\right]} \cos\left(v\frac{\pi}{\tau}x\right), \quad (11)$$

$$B_{s1y} = -\mu_0 \frac{\partial A_{s1}}{\partial y}$$

$$= -\mu_0 \sum_{v=1}^{\infty} \frac{\pi}{v\tau} f_{sv} \frac{\cosh\left[\frac{v\pi}{\tau}(h_m + g - y)\right]}{\sinh\left[\frac{v\pi}{\tau}(h_m + g)\right]} \sin\left(v\frac{\pi}{\tau}x\right). \quad (12)$$

C. Analytical and FEM results of flux density

In this section, the results of the flux density obtained by the analytic method i.e. Maxwell's equation, is compared to those evaluated by the FEM. X and Y components of the air gap flux density distribution are presented as a function of displacement in Fig. 3 and Fig. 4 when the motor is open circuited. Y component of the flux density in the middle of the magnetic air gap is illustrated in Fig. 5.
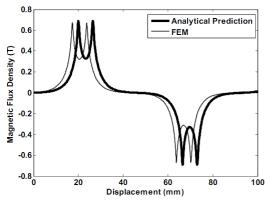

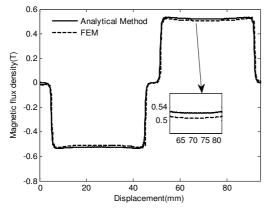Fig. 3. X component of the flux density in the middle of the air gap.

Fig. 4. Y component of the flux density in the middle of the air gap.

Nonlinearity and saturation of the iron core are considered by FEM analysis using the corresponding B-H curves of the ferromagnetic materials. In addition, structural complexity such as slotting can be simply simulated by FEM. As depicted in Figs. 3 and 4, the results obtained by the analytic

method and FEM are nearly similar.

In the ACPMLSM, the effective length of the magnetic air gap is large. Therefore, as shown in Figs. 4 and 5, the distributions of the Y-axis component of the air gap flux density in the middle of the mechanical and magnetic air gap, are nearly rectangular and sinusoidal, respectively. The flux lines of the motor are shown in Figs. 6.

Assuming balanced three-phase currents where $I_a = 2 \times \cos(\omega t)$, currents for the time $\omega t = 0$ will be $I_a = 2$, $I_b = I_c = -1$.
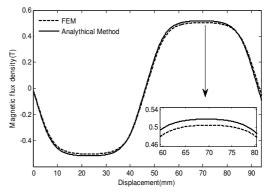

Fig. 5. Y component of the flux density in the middle of the magnetic air gap.
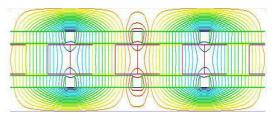

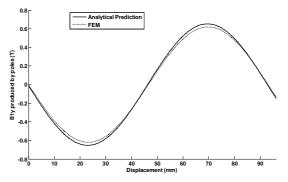Fig. 6. Flux lines at the center of the motor.

Fig. 7. The first harmonic of vertical component of the air gap flux density produced by the PM using analytical method and FEM.
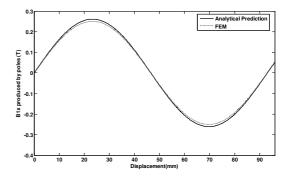

Fig. 8. The first harmonic of horizontal component of the air gap flux density produced by the PM using analytical method and FEM.

Fig. 7 to Fig. 9 illustrate a few samples of the first

harmonic of the vertical and horizontal air gap flux densities generated individually by the PMs and primary currents which are evaluated using Maxwell's equations and FEM. As seen in the figures, the air gap flux density is mainly produced by the PM. Also a comparison between the first harmonics of the flux densities calculated by the analytical model and evaluated by FEM reveals the validity of the analytical modeling approach of the flux densities.
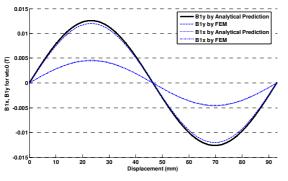

Fig. 9. The vertical and the horizontal components of the air gap flux density generated by the primary currents at ωt=0 using analytical method and FEM.

III. BASIC EQUATIONS OF SYNCHRONOUS MOTOR

The phasor diagram of a synchronous motor is shown in Fig. 10. The following equations are deduced from the vector diagram of Fig. 10 [1]:

$$V_1 \sin \delta = -i_d R_1 + i_q X_{sq}, \tag{13}$$

$$V_1 \cos \delta = i_q R_1 + i_d X_{sd} + E_f, \tag{14}$$

where δ is the load angle which is the angle between the terminal phase voltage V_1 and the no-load voltage E_f. Parameters X_{sd} and X_{sq} are the d and q axis reactance respectively, and R_1 is the resistance per phase of the primary winding.
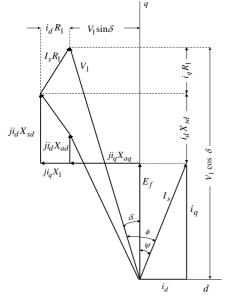

Fig. 10. The vector diagram of the synchronous motor.

According to (13) and (14), the d and q currents are as below [1]:

$$i_d = \frac{V_1(X_{sq} \cos \delta - R_1 \sin \delta) - E_f X_{sq}}{X_{sd} X_{sq} + R_1^2}, \tag{15}$$

$$i_q = \frac{V_1(R_1 \cos \delta + X_{sd} \sin \delta) - E_f R_1}{X_{sd} X_{sq} + R_1^2}. \tag{16}$$

The rms value of the primary current can be evaluated versus V_1, E_f, X_{sd}, X_{sq}, δ and R_1 using

$$I_s = \sqrt{i_d^2 + i_q^2}. \tag{17}$$

A. Thrust calculation

Enduring d-q model of the machine in a synchronously rotating reference frame is used for the optimal design purposes. In this model, the iron saturation is neglected and the flux density distribution along the air gap assumed to be sinusoidal. Therefore, the motor thrust can be calculated by [12]

$$F_{av} = \frac{3}{2} \frac{\pi}{\tau} \left(\lambda_{PM} + \left(L_d - L_q \right) i_d \right) i_q, \tag{18}$$

in which λ_{PM} is the linkage flux per phase caused by the PMs and L_d and L_q are the d axis and q axis inductances, respectively. For a PM motor made by the rare earth materials, the relative permeability is somewhat equal to 1 and thus the material is far to be saturated so that $L_d \approx L_q$. A small difference between L_d and L_q yields to a small component of the reluctance force which is neglected here. Therefore, the mean value of the thrust is simply written as

$$F_{av} = \frac{3}{2} \frac{\pi}{\tau} \lambda_{PM} i_q. \tag{19}$$

B. Losses calculation

For an ACPMLSM, the resistance of the primary winding is considerable compared with the leakage reactance. The copper loss of an ACPMLSM is obtained by

$$P_{cu} = 3R_1 I_s^2. \tag{20}$$

Iron loss consists of the hysteresis loss and eddy-current loss. It can be estimated using [13]

$$P_t = P_h + P_e = k_h B_m^{\beta} f + k_e B_m^2 f^2, \quad [W/m^3], \tag{21}$$

where B_m is the maximum flux density, k_h, k_e and β are constants. Constant parameter β has a value from 1.8 to 2.2 depending on the laminated materials. Variations of the flux density in the yoke can be approximated by Fig. 11.
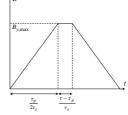

Fig. 11. Flux density variations in the yoke [14].

At the first stage of designing, an initial estimated value is chosen for the maximum flux density of the yoke. The eddy-current loss density of the yoke is expressed as [14]

$$P_{ey} = 8k_e \frac{\tau}{\tau_p} \left(\frac{v_s}{\tau} B_{y,\max} \right)^2, \quad [W/m^3], \qquad (22)$$

where v_s is the linear speed and $B_{y,\max}$ is the maximum value of the yoke flux density as shown in Fig. 11. In (22), the longitudinal component of the eddy-current loss has been ignored. This component is simply taken into account by a constant k_c with the value chosen within 1.1 to 1.2 [14]. The eddy-current loss of the motor is then written as [14]

$$P_e = 8k_e k_c \frac{\tau}{\tau_p} (\frac{v_s}{\tau} B_{y,\max})^2 \times V_y (W). \qquad (23)$$

C. Efficiency calculation

Given the motor losses and the output power, the efficiency is calculated as follows

$$\eta = \frac{P_{out}}{P_{out} + P_{cu} + P_{add} + P_t}, \qquad (24)$$

in which $P_{out} = F_{av} \cdot v_s$ is the output power and P_{add} is the additional losses consisting the mechanical and stray losses.

IV. OPTIMIZATION

The optimization problem with n number of variables, m number of constraints and the objective function $f(x)$, is defined as [15]

$$Maximize \quad f(x), x \in K, \qquad (25)$$

where the parameter K is defined as

$$K = \left\{ x \in R^n : g_i(x) \le 0, \quad i = 1, 2, ..., P \right\}. \qquad (26)$$

In the previous equation $g_i(x)$ determines the limits of the design variables. The design parameters are optimized considering the objective functions defined such as thrust per volume or mass maximization, volume of the PM minimization and power per volume or mass maximization. In this paper, the design parameters are optimized for the efficiency maximization using the genetic algorithm.

For the purpose of maximizing the efficiency of the motor, four design variables are optimized. These four variables are height of the PM, air-gap, height of the primary winding and height of the secondary yoke. The width of the motor, current density and pole pitch are assumed constants specified properly.

A. Constraints

Thermal stress and demagnetizing boundary of the PMs are considered as constraints. In addition, to prevent saturation of the yoke, the minimum values of its dimensions are considered.

The thermal stress which depends on the total losses of the motor is given as [16]

$$\Delta T = \frac{\sum losses}{h S_{TH}} \le \Delta T_{\max}, \qquad (27)$$

where h, S_{TH} and $\Delta T_{\max}$ are the heat exchange coefficient of the surface, heat exchange or cooling surface and maximum rise of the operating temperature, respectively.

Maximum flux density produced by the primary currents, B_s has to be smaller than the value that demagnetizes the PMs. B_s is given by [16]

$$B_s = \frac{3}{2} \frac{4\mu_0 k_{w1} N_1}{g \pi} I_s \sqrt{2}. \qquad (28)$$

To avoid demagnetizing the PMs, primary currents must be limited so that [16]

$$B_s \sin \alpha \le \left(\frac{h_m}{g_e} B_r - B_D \right), \qquad (29)$$

where B_D is the critical or minimum allowable magnetic flux density of the PMs. The value of B_D is about -0.2 tesla for the Nd-Fe-B magnet.

A minimum value for the height of the secondary yoke can be obtained by using the following equation

$$h_{y,\min} = \frac{B_{1g}}{B_{y,\max}} \tau. \qquad (30)$$

B. Simulation results of optimization

As mentioned earlier, efficiency maximization is the objective of the optimization problem of this paper. The rated power P_{out} and linear speed v_s of the motor are assumed 1000 W and 4.65 m/s at 50 Hz supply frequency respectively. The additional loss is assumed 4% of the output power. The design variables and their variations ranges are listed in Table II. The temperature limit of the motor is assumed 100 °C and the heat exchange coefficient of the surface is assumed h=24.6 (W/m²°C). The maximum flux density of the yoke is $B_{y,\max} = 1.4$ tesla.

Optimized design variables obtained by the genetic algorithm are given in Table III. The results show that the efficiency of the optimized motor has been increased by 4.23% in comparison with the initial design. Also, despite the copper loss has reduced by 59.7%, the iron loss has increased by 140%. However, the influence of the copper loss on the efficiency is more than that of the iron loss, so the efficiency of the optimized machine is higher.

Harmonic contents of the flux density produced by the PMs are evaluated using FEM. These Harmonics for the initial design and optimized machine are shown in Fig. 12.

The amplitude of the first harmonic of the flux density before and after the optimization is 0.62 and 0.78 Tesla, respectively showing an increase of the flux density for the optimized machine. However, as expected an increase of the

flux density yields to a higher iron loss.

TABLE II. DESIGN VARIABLES AND THEIR VARIATION RANGES.

Parameter (unit)	Min.	Max.
Air gap length (mm)	0.5	1
Height of the PM (mm)	4	7
Height of the secondary yoke (mm)	5	30
Height of the winding (mm)	5	15

TABLE III. PARAMETERS OF THE OPTIMIZED MACHINE.

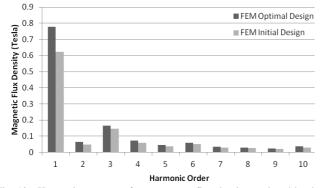| Parameter (unit)	Initial design	GA output
Air gap length (mm)	0.5	0.51
Height of the PM (mm)	5	7
Height of the secondary yoke (mm)	10	26.2
Height of the winding (mm)	12	10
Cupper loss (W)	103	41.5
Iron loss (W)	6	14.1
Efficiency	87	91.23

Fig. 12. Harmonic contents of y component flux density produced by the PMs before and after optimization.

V. CONCLUSIONS

A modeling and optimally design procedure of the air-core double-sided permanent magnet linear synchronous motor are presented in this paper. Flux density, MMF and other parameters of motor are calculated using the Maxwell's equations based analytical model. The results obtained from the analytical model are compared with those obtained from the FEM. This comparison confirms the accuracy of the presented model. Therefore the analytical model proposed in this paper can be applied for analysis, design and optimization of the ACPMLSM with some confidence. At the last section of the paper, a maximum efficiency of ACPMLSM is optimally designed using the proposed model coupled with genetic algorithm based optimization approach. The simulation results of the optimally designed motor indicate that the iron loss increases by more than 140% due to the increasing of the first harmonic of the flux density from 0.62 to 0.78 tesla. Although the iron loss increases, the copper loss reduces up to 60%. Since the copper loss has more effect on the efficiency, the overall efficiency of the optimally designed motor is increased.

REFERENCES

[1] J. G. Gieras, Z. J. Pich, *Linear Synchronous Motors*. Boca Raton, FL: CRC, 2000.

[2] I. Boldea, S. A. Nasar, *Linear Electromagnetic Devices*. New York. Taylor & Francis, 2001.

[3] G. H. Kang, J. P. Hong, G. T. Kim, "Design and analysis of slotless type permanent magnet linear brushless motor by using equivalent

magnetizing current", *IEEE Trans. on Magnetics*, vol. 37, pp. 1241–1247, Sept. 2001.

[4] N. Chayopitak, D. G. Taylor, "Performance assessment of air–core linear permanent–magnet synchronous motors", *IEEE Trans. on Magnetics*, vol. 44, pp. 2310–2316, Oct. 2008. [Online]. Available: http://dx.doi.org/10.1109/TMAG.2008.2002259

[5] K. C. Lim, J. K. Woo, G. H. Kang, J. P. Hong, G. T. Kim, "Detent force minimization techniques in permanent linear synchronous motors", *IEEE Trans. on . Magnetics,* vol. 38, pp. 1157–1160, Mar. 2002. [Online]. Available: http://dx.doi.org/10.1109/20.996296

[6] M. Inoue, H. Sato, "An approach to a suitable stator length for minimization the detent force of permanent magnet linear synchronous motors", *IEEE Trans. on. Magnetics,* vol. 36, no. 4, pp. 1890–1893, July 2000. [Online]. Available: http://dx.doi.org/10.1109/20.877814

[7] A. Hassanpour Isfahani, S. Vaez–Zadeh, "Design optimization of a linear permanent magnet synchronous motor for extra low force pulsation", *Journal of Energy Conversion and Management,* vol. 48, pp. 443–449, 2007. [Online]. Available: http://dx.doi.org/10.1016/j.enconman.2006.06.022

[8] G. H. Kang, J. P. Hong, G. T. Kim, "A novel design of an air–core type permanent magnet brushless motor by space harmonic field analysis", *IEEE Trans. on Magnetics,* vol. 37, pp. 3732–3736, Sept. 2001. [Online]. Available: http://dx.doi.org/10.1109/20.952701

[9] D. H. Im, J. P. Hong, I. S. Jung, S. B. Yoon, "The optimum design of permanent magnet linear synchronous motor", *in Proc. of IEEE CEFC 96*, pp.166–172, 1996.

[10] S. Vaez–Zadeh, A. Hassanpour Isfahani, "Multi–objective design optimization of air–core linear permanent magnet synchronous motors for improved thrust and low magnet consumption", *IEEE Trans. on Magnetic*, vol. 42, pp. 446–452, Mar. 2006. [Online]. Available: http://dx.doi.org/10.1109/TMAG.2005.863084

[11] J. Wang, M. West, D. Howe, H. Zelaya, W. M. Arshad, "Design and experimental verification of a linear permanent magnet generator for a free–piston energy convertor", *IEEE Trans. on Energy conversion,* vol. 22, pp. 299–307, June 2007.

[12] Z. Q. Zhu, D. Howe, "Instantaneous magnetic field distribution in brushless permanent magnet dc motor, part III: effect of stator slotting", *IEEE Trans. on Magnetics,* vol. 29, pp. 143–151, Jan. 1993. [Online]. Available: http://dx.doi.org/10.1109/20.195559

[13] C. Mi, G. R. Slemon, R. Bonert, "Modeling of iron losses of permanent–magnet synchronous motors", *IEEE Trans. Ind. App.*, vol. 39, pp. 734–742, May/Jun. 2003. [Online]. Available: http://dx.doi.org/10.1109/TIA.2003.810635

[14] B. Sheikh–Ghalavand, S. Vaez–Zadeh, A. Hassanpour Isfahani, "An improved magnetic equivalent circuit model for iron–core linear permanent magnet synchronous motor", *IEEE Trans. on Magnetics,* vol. 46, Jan. 2010.

[15] N. Bianchi, S. Bolognani, "Analytical optimization of inset permanent magnets machine based on a genetic algorithm", *Electrical Machines and Power Electronics*, pp. 440–445, Sept. 2007.

[16] T. Sebastian, G. Slemon, "Transient modeling and performance of variable–speed permanent–magnet motors", *IEEE Trans. Ind. App.*, vol. 25, pp. 101–106, Jan/Feb. 1989. [Online]. Available: http://dx.doi.org/10.1109/28.18878